HHS Public Access

Author manuscript

J Bone Miner Res. Author manuscript; available in PMC 2024 December 01.

Published in final edited form as:

J Bone Miner Res. 2023 December ; 38(12): 1834–1845. doi:10.1002/jbmr.4915.

VEGF Secretion Drives Bone Formation in Classical MAP2K1+ Melorheostosis

Jules Allbritton-King[1,2], **Jyotirindra Maity**[1], **Amit Patel**[1], **Robert A Colbert**[3], **Fatemeh Navid**[3,*], **Timothy Bhattacharyya**[1,*]

[1]Clinical and Investigative Orthopedics Surgery Unit, National Institute of Arthritis and Musculoskeletal and Skin Diseases, National Institutes of Health, Bethesda, Maryland, USA

[2]Current address: Harvard-MIT Division of Health Sciences and Technology, Harvard Medical School, Boston, Massachusetts, USA

[3]Pediatric Translational Research Branch, National Institute of Arthritis and Musculoskeletal and Skin Diseases, National Institutes of Health, Bethesda, Maryland, USA

Abstract

Patients with classical melorheostosis exhibit exuberant bone overgrowth in the appendicular skeleton, resulting in pain and deformity with no known treatment. Most patients have somatic, mosaic mutations in *MAP2K1* (encoding the MEK1 protein) in osteoblasts and overlying skin. As with most rare bone diseases, lack of affected tissue has limited the opportunity to understand how the mutation results in excess bone formation. The aim of this study was to create a cellular model to study melorheostosis.

We obtained patient skin cells bearing the *MAP2K1* mutation (affected cells), and along with isogenic control normal fibroblasts reprogrammed them using the Sendai virus method into induced pluripotent stem cells (iPSCs). Pluripotency was validated by marker staining and embryoid body formation. iPSCs were then differentiated to mesenchymal stem cells (iMSCs) and validated by flow cytometry. We confirmed retention of the *MAP2K1* mutation in iMSCs with PCR and confirmed elevated MEK1 activity by immunofluorescence staining.

Mutation-bearing iMSCs showed significantly elevated VEGF secretion, proliferation and collagen I and IV secretion. iMSCs were then differentiated into osteoblasts, which showed increased mineralization at 21 days and increased VEGF secretion at 14 and 21 days of differentiation. Administration of VEGF to unaffected iMSCs during osteogenic differentiation was sufficient to increase mineralization. Blockade of VEGF by bevacizumab reduced mineralization in iMSC-derived affected osteoblasts and in affected primary patient-derived osteoblasts.

These data indicate that patient-derived induced pluripotent stem cells recreate the elevated MEK1 activity, increased mineralization, and increased proliferation seen in melorheostosis patients. The

Corresponding Author:Dr. Timothy Bhattacharyya, Clinical and Investigative Orthopedic Surgery Section, 10 Center Drive, Bldg. 10-CRC, Room 4-2339, MSC1498, Bethesda, Maryland 20892, 301-443-8388.

*equal contributions

Disclosure Statement:

The authors have no conflicts of interest to declare.

increased bone formation is driven, in part, by abundant VEGF secretion. Modifying the activity of VEGF (a known stimulator of osteoblastogenesis) represents a promising treatment pathway to explore. iPSCs may have wide applications to other rare bone diseases.

Keywords

Melorheostosis; iPSCs; Osteoblasts; VEGF; Mineralization

INTRODUCTION

Rare bone-forming diseases provide a window into bone biology that can have profound implications. Investigation into the rare disease sclerostosis resulted in discovery of sclerostin, which led to the osteoporosis treatment romosozumab [(1)].

Patients with melorheostosis exhibit exuberant bone overgrowth, usually in one arm or leg (Figure 1) [(2–4)]. In classical melorheostosis, bone lesions are metabolically active on ^{18}F-NaF scans and have a characteristic “dripping candlewax” appearance on radiographs [(5,6)]. In approximately 30% of patients, skin overlying affected bone is thickened and erythematous [(7)]. Histology of melorheostosis reveals dense, lamellar bone overgrowth along the periosteal surface that subsequently undergoes intense remodeling, whereas affected skin is characterized by increased blood vessel density and thickness [(5,7)]. While melorheostotic lesions do not metastasize, bone overgrowth continues throughout the patient’s life. There is no known treatment.

Most cases of classical melorheostosis are caused by somatic, mosaic mutations (Q56P, K57N, or K57E) clustered in the negative regulatory domain of *MAP2K1* [(5)]. These mutations result in a loss of the negative regulatory domain’s inhibitory role in the encoded MEK1 protein. The resulting MEK1 protein variant exhibits kinase activity on its downstream targets, ERK1 and ERK2, in the absence of upstream RAF1 signaling [(8–13)]. Recently, our group has implicated elevated VEGF secretion and ECM production in mutation-bearing melorheostotic fibroblasts in the abnormal angiogenesis observed in affected skin [(14)]. However, how *MAP2K1* activating mutations lead to bone overgrowth is unknown.

As with other rare bone diseases, limited availability of affected bone limits the ability to investigate pathogenesis. While human bone can be obtained surgically for research purposes, it requires full anesthesia and a control sample. To circumvent these limitations, we established an iPSC-derived model of the melorheostosis. We use this model to show that *MAP2K1* mutations result in increased VEGF secretion that, in part, drives increased osteoblast mineralization.

MATERIALS AND METHODS

Dermal Fibroblast Isolation

Dermal fibroblasts were isolated from shaved skin biopsies from patients with melorheostosis performed in accordance with NIAMS Institutional Review Board-approved

protocol (NCT02504879). Biopsies were collected from affected skin with characteristic dermatological abnormalities, as well as contralateral unaffected skin from the same patient. Skin biopsies were briefly submerged in 70% ethanol, rinsed twice with PBS, and then incubated in dispase solution at 4° C overnight. The epidermis and subcutaneous fat were removed from the dermis, and the dermis was placed onto a tissue culture dish and briefly allowed to dry in order to adhere to the culture surface. The dermal biopsy was then incubated in fibroblast growth medium (DMEM supplemented with 10% fetal bovine serum (FBS, Gibco) and 1% Penicillin/Streptomycin (P/S, Gibco)) for up to three weeks, or until fibroblasts expanded from the dermis onto the culture surface. Droplet digital PCR (ddPCR) for melorheostosis-associated *MAP2K1* mutations was used as previously described[14] to verify the mutation's presence or absence in affected and unaffected cells, respectively.

Induced Pluripotent Stem Cell (iPSC) Generation and Validation

Affected (carrying *MAP2K1* mutation, as verified by digital droplet PCR) and unaffected patient fibroblasts at passage 9 were expanded, tested for mycoplasma, and reprogrammed using Sendai virus transduction, as described before [15]. Briefly, Cytotune 2 (Thermo# A16517) Sendai virus kit was used to infect 50,000 fibroblast cells with 5ul premixed SeVs (1:1:1 ratio of three SeVs, MOI=3:3:3) in DMEM+10% FBS. 4 days after infection, fibroblast cells were dissociated using Trypsin and replated onto 48-well Matrigel-coated plate by serial dilution to 50–5,000 cells/well and cultured with reprogramming medium (E8 medium without bFGF, Gibco) for 20 days. Medium was switched to E8 after day 20. 12 iPSC closed were picked based on morphology. Six iSPC lines that maintained growth rate and morphology were expanded in passage two. An iPSC-like single colony in a well was passaged using 0.5mM EDTA/DPBS and expanded to establish iPSC clone [16]. Expression of two pluripotency markets (TRA-1–60 and NANOG) were confirmed by flow cytometry. While multiple patients samples were carried through the iPSC induction process, only a line from one patient maintained the mutation and pluripotency.

Routine iPSC culture was performed as previously described [17]. Briefly, iPSCs were cultured on 6-well plates coated with 0.16 mg/mL Matrigel (Corning) using StemFlex feeder-free iPSC medium (Gibco). Medium was changed every 2 days. Cells were passaged at 70–80% confluence by gentle dissociation in 0.5 mM EDTA in PBS followed by re-seeding on fresh Matrigel-coated plates in StemFlex with 1x RevitaCell supplement (Gibco). The day after passaging, medium was removed and replaced with StemFlex without RevitaCell supplementation. iPSCs were expanded to passage 15+ prior to downstream experimentation, and genetic integrity was confirmed via G-banded karyotyping (WiCell).

Pluripotency was assessed by immunofluorescent staining for OCT4, SSEA4, and TRA-1–60, as well as embryoid body formation. For pluripotency marker staining, iPSCs were expanded to 80% confluence and fixed with 4% formaldehyde in PBS for 20 min at room temperature, then rinsed thrice with PBS. Fixed iPSCs were blocked with 10% normal goat serum (Life Technologies) + 0.1% Triton X-100 (AmericanBio) in PBS for 10 min at room temperature, then rinsed thrice with PBS. Cells were then incubated overnight at 4° C in a 1:50 dilution of fluorophore-linked antibodies for either OCT4 (Millipore), SSEA-4

(BioLegend), or TRA-1–60 (BioLegend). The following day cells were rinsed with PBS and counterstained with 10 μg/mL DAPI (Sigma) for 10 min at room temperature in PBS.

For embryoid body formation, iPSCs were passaged as normal and transferred to a 6-well low-attachment plate in StemFlex supplemented with 1x RevitaCell. The day after plating, medium was exchanged for Embryoid Body medium (DMEM supplemented with 20% FBS) and cells were cultured for 10 days. By day 10, cells had self-aggregated into spheroids. Spheroids were then gently transferred to a Matrigel-coated 12-well plate and cultured for an additional 14 days in Embryoid Body medium, changing medium every 2 days. Spheroids were fixed with 4% formaldehyde in PBS for 20 min at room temperature, rinsed thrice with PBS, then blocked in 5% normal goat serum + 0.3% Triton X-100 in PBS for 1 hr at room temperature. Spheroids were then incubated overnight at 4° C in a 1:100 dilution of germ-layer specific primary antibodies for either α-Fetoprotein (R&D Systems), α-Smooth muscle actin (Novus Biologicals), or β-III Tubulin (R&D Systems). Spheroids were rinsed thrice in 0.1% BSA in PBS, then incubated for 1 hr at room temperature in a 1:500 dilution of Alexa-488 Goat anti-Mouse IgG (Invitrogen). Spheroids were then rinsed with PBS and counterstained with DAPI.

Mesenchymal Stem Cell (iMSC) Differentiation and Culture

Affected and unaffected iPSCs were differentiated into iMSCs using the STEMdiff Mesenchymal Progenitor Kit (StemCell Technologies) per the manufacturer's protocol. Briefly, iPSCs were cultured to 30–50% confluency and medium was exchanged for STEMdiff-ACF Mesenchymal Induction Medium. Medium was changed daily for 3 days, then exchanged for complete MesenCult-ACF Plus Medium, changed daily. At day 6, cells were dissociated with 0.5 mM EDTA solution and plated on 6-well plates coated with Animal Component-Free Cell Attachment Substrate. Half-medium changes were performed daily, and cells were passaged at 80% confluency. At day 21, cells were dissociated with TrypLE Express (Gibco) and transferred to tissue culture flasks and cultured in iMSC medium α-MEM supplemented with 15% FBS (Millipore) and 1% P/S.

Flow Cytometry of iPSC-derived MSCs

To evaluate cell surface expression of a defined iMSC-specific panel of markers, iMSCs were dissociated with TrypLE Express, blocked for 30 min at 4° C in 3% BSA in PBS, and then 200,000 cells per well were incubated for 30 min at 4° C with fluorophore-linked antibodies for positive staining: PE-CD90, PE-CD44, PE-CD73, PE-CD105 or negative staining: PE-CD34, PE-CD14, PE-CD19, PE-CD45, PE-HLA-DR (PE-CD44: BD Biosciences, all others BioLegend). Cells were rinsed twice with PBS, resuspended in ice-cold 1% BSA in PBS, and assessed using an Attune NxT Flow Cytometer (Thermo Fisher). Bone-marrow derived iMSCs (ATCC) were used as a positive control for iMSC flow cytometry. Groups were run in parallel with PE Mouse IgG1, k and PE Mouse IgG2b, k (BioLegend) as isotype controls.

pERK1/2 Immunocytochemical Staining

To assess ERK1/2 phosphorylation by MEK1 in affected and unaffected cells, iPSCs were cultured as normal, serum-starved for 1 hr in basal StemFlex medium with no added

supplement, and then stimulated for 5 min in complete StemFlex medium supplemented with 5% FBS. iMSCs were serum-starved in the same manner with basal α-MEM and stimulated with iMSC medium. Cells were fixed in 4% formaldehyde in PBS for 15 min at room temperature, rinsed thrice with PBS, and permeabilized in ice-cold methanol for 10 min at −20° C. Cells were blocked in 5% normal goat serum + 0.3% Triton X-100 in PBS for 1 hr at room temperature, then incubated overnight at 4° C in a 1:250 dilution of rabbit-anti-pERK1/2 (Cell Signaling Technology) in 1% BSA + 0.3% Triton X-100 in PBS. The next day, cells were incubated for 2 hrs at room temperature in a 1:500 dilution of Alexa-488 goat anti-rabbit secondary antibody (Invitrogen), rinsed with PBS, and counterstained with DAPI.

VEGF Secretion

Measurement of VEGF secretion by affected and unaffected iMSCs and osteoblasts was conducted by plating 200,000 cells/well in a 6-well plate in iMSC medium. The following day, cells were serum-starved in basal α-MEM for 2 hours. Medium was then exchanged for α-MEM supplemented with 5% FBS with or without 10 μM trametinib. After 48 hours, cell supernatants were collected and VEGF secretion was quantified using the Human VEGF Quantikine ELISA Kit (R&D Systems) according to the manufacturer's protocol. VEGF secretion by iMSCs during osteogenic differentiation was assessed at 7, 14, and 21 days in the same manner.

VEGF Expression Analysis

For assessment of VEGF mRNA expression in affected and unaffected iMSCs, 100,000 cells/well were seeded in 6-well plates in MSC medium. The following day, cells were serum-starved in basal α-MEM for 2 hours. Medium was then exchanged for α-MEM supplemented with 5% FBS with or without 10 μM trametinib. After 48 hours, cells were lysed from culture plates using TRIzol and RNA was extracted using the Direct-zol RNA kit (Zymo Research) according to the manufacturer's protocol. RNA concentration and purity was verified using a NanoDrop spectrophotometer (Thermo Fisher) and complementary DNA (cDNA) was synthesized using the iScript kit (Bio-Rad) according to the manufacturer's protocol, using 500 ng starting RNA. Real-time quantitative polymerase chain reaction (qPCR) was performed using a QuantStudio 6 Flex PCR System (Thermo Fisher) using the VEGFA TaqMan primer and TaqMan Master Mix (Thermo Fisher). Amplification data was processed using the $2^{-\Delta\Delta Ct}$ method as previously described.

MSC Proliferation

To measure the relative proliferation rates of affected and unaffected iMSCs, 5,000 cells/well were seeded in 96-well plates in MSC medium. At 24, 48, and 72 hours, cells were incubated in 1 ug/mL Hoechst 33342 (Thermo Fisher) in MSC medium for 15 minutes at 37° C. Medium was exchanged for normal MSC medium, and cells were imaged and counted using a Celigo 5-channel Imaging Cytometer (Nexcelom Bioscience). Cell proliferation was also measured with Ki-67 staining[18]. We seeded affected and unaffected iMSCs, 7000 cells/well in 8-well chamber slide in MSC medium and media was changed every third day. At day 6 cells were processed for immunocytochemical staining. Cells were washed with 1XPBS and fixed in 4% formaldehyde in PBS for 20 min at room temperature,

rinsed thrice with 1X PBS, and permeabilized with 0.25% Triton X-100 for 30 min on ice. Cells were blocked in 10% normal goat serum + 0.1% Triton X-100 in PBS for 30 min at room temperature, then incubated overnight at 4°C in a 1:200 dilution of mouse-anti-Ki-67 conjugated with Alexa Fluor 647 (BioLegend) in 1% BSA + 0.3% Triton X-100 in PBS. The next day, cells were washed three times with 1X PBS, and counterstained with Hoechst dye to visualize nuclei. Cells were imaged and counted using 40X magnification of Leica DM6000 microscope and iVision-MAC software.

ECM Secretion

To assess ECM deposition by affected and unaffected iMSCs, 150,000 cells/well were plated in 6-well plates in MSC medium. The following day, medium was exchanged for pro-ECM medium (α-MEM supplemented with 15% FBS, 1% P/S, and 1.36 μM ascorbic acid). Pro-ECM medium was changed three times per week. After 14 days, cells were fixed in 4% formaldehyde in PBS for 15 min at room temperature, rinsed thrice with PBS, and blocked in 10% FBS in PBS for 1 hr at room temperature. Cells were then incubated in a 1:250 dilution of either rabbit-anti-Collagen I (abcam) or rabbit-anti-Col4A2 (abcam) in 1% BSA overnight at 4° C. The next day, cells were incubated for 1 hr at 4° C in a 1:500 dilution of Alexa-488 goat anti-rabbit secondary antibody (Invitrogen), rinsed with PBS, and counterstained with DAPI.

Patient Bone Samples

Bone samples were collected from three patients who underwent surgical removal of painful or ankylosed areas of melorheostosis overgrowth. Primary affected bone samples were cultured as previously described [(5)]. Because most cells in affected bone are mutation negative, we divided the bone into various pieces. After cell expansion in culture, we identified osteoblasts that were mutation negative by ddPCR and these cultures were used as unaffected controls. For one patient (Melo 52), unaffected control bone was obtained from the contralateral iliac crest. Note that the bone samples did not come from patients whose skin fibroblasts were reprogrammed into iPSCs.

VEGF Immunohistochemical Staining

Slides were baked at 60°C for 1hr then subsequently deparaffinized and rehydrated. Antigen retrieval was performed using EDTA buffer for 17 hr at 60°C. Following antigen retrieval, VEGF staining was performed using a Leica Bond RX autostainer (Leica). Anti-VEGF antibody (R&D Systems) was diluted to 1:100 with a 30 min incubation time on the tissue. Antibody detection was accomplished using a Rabbit anti-Goat secondary antibody (Vector Laboratories) at a 1:500 dilution, followed by Streptavidin-HRP (Invitrogen) diluted to 1.4 ug/ml. Prior to primary antibody application, additional blocking steps to reduce background staining were performed. This included the application of Avidin/Biotin blocking reagents (Vector Laboratories) followed by 10% Normal Goat Serum for 20mins. DAB chromogen and hematoxylin counterstain were provided by the Bond Polymer Refine detection kit (Leica). Normal Human Pancreas was used as a positive control (Pantomics).

Osteogenic Differentiation

To assess the osteogenic potential of affected and unaffected cells, iMSCs or primary osteoblasts were seeded at 30,000 cells/well in 6-well plates in normal MSC medium. The following day, medium was exchanged for osteogenic medium (α-MEM supplemented with 15% FBS, 1% P/S, 10 mM β-glycerophospate (Millipore Sigma), 50 μg/mL ascorbic acid (Millipore Sigma), and 100 nM dexamethasone (Millipore Sigma)). Osteogenic medium (OS^+) was changed every third day. At 7, 14, and 21 days, cell supernatants were collected for ELISA analysis and cells were fixed with 4% formaldehyde in PBS for 15 min at room temperature, rinsed with DI H2O, and incubated in 2% Alizarin Red solution for 60 min at room temperature. Alizarin Red solution was removed, and cells were gently rinsed twice with DI H2O prior to imaging. For quantification, Alizarin Red stain was dissolved in 10% Cetylpyridinium chloride (CPC), 10 mM Na_2PO_4 solution (Millipore Sigma). The extracted dye was measured at 560 nm using a Synergy HT spectrophotometer (Bio-Tek).

Osteogenic Gene Expression

For assessment of osteogenic gene expression in iMSCs, cells were seeded at 30,000 cells/well in 6-well plates in MSC medium. The following day, medium was exchanged wither either MSC medium or osteogenic medium (α-MEM supplemented with 10% FBS, 1% P/S, 10 mM β-glycerophospate (Millipore Sigma), 50 μg/mL ascorbic acid (Millipore Sigma), and 100 nM dexamethasone (Millipore Sigma)). Medium was changed every third day. At 14 days, cells were lysed using TRIzol and RNA was extracted using the Direct-zol RNA kit (Zymo Research) according to the manufacturer's protocol. RNA concentration and purity was verified using a NanoDrop spectrophotometer (Thermo Fisher) and complementary DNA (cDNA) was synthesized using the iScript kit (Bio-Rad) according to the manufacturer's protocol, using 500 ng starting RNA. Real-time quantitative polymerase chain reaction (qPCR) was performed with a QuantStudio 6 Flex PCR System (Thermo Fisher) using the *RUNX2*, *COL1A1*, and *ALPL* TaqMan primer and TaqMan Master Mix (Thermo Fisher). Amplification data was processed using the $2^{-\Delta\Delta Ct}$ method as previously described.

Anti-VEGF treatment

To assess the effect of VEGF neutralization on osteogenic differentiation of affected and unaffected iMSCs or primary osteoblasts, cells were seeded at 30,000 cells/well in 6-well plates in normal MSC medium (OS^-). The following day, medium was exchanged for osteogenic medium (OS^+) with or without 2 μg/ml bevacizumab (anti-VEGF mAb, Selleckchem).OS^+ was changed with or without bevacizumab every third day up to 21 days. After harvesting, cells were fixed and stained with Alizarin Red to evaluate mineralization.

Statistical Analysis

Experiments were conducted on all patient cell lines with both unaffected and affected cell lines available (n = 1 iPSC line, n = 2 primary osteoblast lines (Melo 32, Melo 52)) in technical triplicate. All statistical analysis was performed on Prism 8.0 software (GraphPad). Data from Figures 3A, 3B, and 3C were analyzed by two-way ANOVA with Sidak's multiple comparisons test, and data from Figure 5B were analyzed by one-way

ANOVA with Tukey's post-hoc test. Comparisons of only two groups were compared using Student's t-test or Mann-Whitney U test depending on normality of data as assessed by the Shapiro-Wilk test. Significance is considered as $p<0.05$. All data is presented as mean ± SD unless otherwise indicated. * = $p<0.05$, ** = $p<0.01$, *** = $p<0.001$, **** = $p<0.0001$.

RESULTS

MAP2K1 mutation-bearing iPSCs are pluripotent and retain elevated ERK activity.

After harvesting affected and unaffected skin fibroblasts overlying melorheostotic bone and reprograming them to iPSCs (Figure 2A), we confirmed the mutation presence by ddPCR (Supplemental Figure 1). Primary affected fibroblasts exhibited a variant allele frequency (VAF) of 0.44 for the K57N mutation, whereas the generated affected iPSCs were clonal and exhibited a VAF of 0.5. Unaffected fibroblasts and iPSCs had a VAF of zero, confirming no mutation present. Chromosomal stability of iPSCs was verified by G-banded karyotyping (Supplemental Figure 2A).

We confirmed pluripotency of the iPSCs by embryoid body formation assay in both unaffected and affected cells, followed by immunofluorescence staining for α-smooth muscle actin, α-fetoprotein, and βIII tubulin to confirm presence of mesoderm, endoderm, and ectoderm respectively (Figure 2B). Both unaffected and affected iPSCs were positive for pluripotency markers OCT4, TRA-1–60, and SSEA4 (Supplemental Figure 2B). Subsequent differentiation of iPSCs to iMSCs was confirmed by flow cytometry for a panel of MSC-specific surface markers as validated against commercially available BM-MSCs (Figure 2C). Like the BM-MSCs, iPSC-derived MSCs were over 90% positive for the surface markers CD44, CD73, CD105, and CD90 and negative for CD19, CD14, CD34, CD45, and HLA-DR.

The downstream action of the *MAP2K1* mutation was observed to cause elevated ERK1/2 phosphorylation in affected primary fibroblasts both with and without FBS stimulation (Figure 2D) as reported previously[14]. To confirm that the *MAP2K1* mutation is present in the reprogramed iPSCs and the iPSC-derived MSCs, cells were stimulated similarly with or without FBS and ERK1/2 phosphorylation was measured. The functionality of the *MAP2K1* mutation was preserved in reprogrammed, affected iPSCs and iMSCs. We observed elevated ERK1/2 phosphorylation even under basal conditions as compared to their unaffected counterparts, which had very low levels of ERK1/2 phosphorylation in the absence of FBS stimulation, suggesting that the MEK1 variant retained its characteristic hyperactive signaling behavior after iPSC reprogramming (Figure 2E-F). Similar to the patient-derived affected fibroblasts, FBS stimulation further increased pERK1/2 levels stronger in both affected iPSCs and iMSCs as compared to their corresponding unaffected controls. Together these results verify that *MAP2K1* mutation and the downstream ERK1/2 increased activation was present in the reprogramed iPSCs and the iPSC-derived MSCs.

MAP2K1 mutation-bearing iMSCs have a proliferative phenotype with increased VEGF secretion.

Since we observed in our previous studies that affected fibroblasts carrying *MAP2K1* mutation secrete increased VEGF[14], we next measured VEGF in the supernatants of the iPSC-derived MSCs. Affected iMSCs cultured for 48h in normal media showed a six-fold increased VEGF release in the supernatant compared to the mutation-free iMSCs (Figure 3A). Furthermore, when affected iMSCs were given the MEK1 inhibitor trametinib, the secretion of VEGF decreased from a mean of 601.2 ± 29.7 pg/mL to 417.2 ±31.2 pg/mL. Interestingly, MEK1 inhibition with trametinib did not affect VEGF levels in supernatants of unaffected iMSCs. Similar findings were observed when studying 48 hour VEGF expression by RT-PCR showing increased VEGF expression in affected iMSCs compared to unaffected cells (Figure 3B). In the presence of trametinib, VEGF expression was significantly downregulated in affected cells compared to unaffected iMSCs. We further confirmed that mutation-bearing primary patient derived osteoblasts secreted higher levels of VEGF and were responsive to trametinib inhibition (Figure 3C)

Affected iMSCs also showed increased proliferation in culture at 24, 48 and 72 h compared to the unaffected controls (Figure 3D). Furthermore, affected iMSCs contained a higher proportion of cells positive for the cell proliferation marker Ki-67 than unaffected iMSCs (Supplemental Figure 5AB). We also observed that affected iMSCs deposited more collagen I and collagen IV when cultured in medium with ascorbic acid (Supplemental Figure 3A–C), as has been previously observed in primary affected fibroblasts [14]. Together these data confirm that *MAP2K1* mutation increases VEGF production in iMSCs and primary osteoblasts similar to primary affected fibroblasts. Further, the MAP2K1 mutation enhances proliferation and ECM deposition of iMSCs.

VEGF is overexpressed in a mosaic pattern in melorheostotic bone lesions.

Since melorheostotic primary osteoblasts showed increased VEGF production, we next analyzed VEGF expression in bone sections of a melorheostosis patient. Immunohistochemical staining of affected bone revealed patchy areas of staining for VEGF, especially near the Haversian canals (Figures 4). Consistent with the mosaic nature of the disease, some osteocytes were positive for VEGF staining interspersed with non-staining osteocytes. These data provide *in vivo* evidence of elevated VEGF signaling in melorheostotic bone lesions in concordance with our findings *in vitro*.

iMSC derived osteoblasts show increased mineralization and VEGF secretion.

Given the excessive bone formation characteristic of melorheostosis, we investigated the mineralization capacity of osteoblasts derived from iMSCs. After 21 days in osteogenic media, affected iMSC-derived osteoblasts exhibited increased mineralization compared to unaffected iMSC-derived osteoblasts, as measured by Alizarin Red staining and spectrophotometric absorbance assay (Figures 5A-B). Markedly increased VEGF secretion was concurrently observed at 14 and 21 days of differentiation in osteogenic medium (Figure 5C). At day 14, affected iMSC-derived osteoblasts showed increased gene expression of osteogenic markers *RUNX2* and *COL1A1* compared to unaffected cells (Supplemental Figure 4). We then confirmed the increased mineralization pattern seen in

iMSC-derived osteoblasts was similar to that seen in primary patient derived osteoblasts carrying *MAP2K1* mutation compared to unaffected cells (Figures 5D-E). At day 14 and 21 of differentiation the primary affected osteoblasts also showed increased mineralization compared to the unaffected controls.

Exogenous VEGF treatment of unaffected iMSC-derived osteoblasts drives mineralization in vitro.

VEGF is a growth factor that can induce mineralization *in vivo*[19]. We then assessed the impact of exogenous VEGF treatment on unaffected iMSCs to further isolate the effect of VEGF on driving mineralization. After 21 days of osteogenic differentiation, we found significantly increased Alizarin red staining in unaffected iMSCs supplemented with 20 ng/mL VEGF (Supplemental Figure 4).

VEGF neutralization reduces mineralization in affected osteoblasts.

In order to further demonstrate a key role for VEGF secretion in melorheostosis, we studied mineralization in the presence of the VEGF inhibitor bevacizumab. We observed that affected iMSCs, that showed increased mineralization compared to unaffected cells at 21 days, showed reduced mineralization in the presence of bevacizumab (Figure 6A). Similarly, two different lines of affected primary osteoblasts mineralized more than paired unaffected osteoblasts at baseline (Figures 6B, C). Quantification by spectrophotometry confirmed that treatment with bevacizumab significantly decreased the total mineralization of affected cells, whereas mineralization of the unaffected cells remained unchanged (Figures 6D, F). Together these data confirm that VEGF is contributing to increased mineralization in melorheostotic cells, suggesting that targeting VEGF might be a therapeutic avenue for treatment.

DISCUSSION

VEGF is understood to mediate bone formation and repair through both direct and indirect means. In this study, we establish an iPSC-based model of pathologic MEK1 activation in mutation-bearing osteoblasts and provide evidence for the role of VEGF secretion in driving increased mineralization. Specifically, we demonstrate elevated VEGF secretion and in patient-derived melorheostosis iMSCs and primary osteoblasts, which is attenuated by MEK1 inhibition. We also confirm enhanced mineralization in affected cell lines, which is rescued by VEGF neutralization.

Interestingly, previous studies have shown that only about 3–30% of osteoblasts within melorheostotic bone lesions bear the disease-causing MAP2K1 variant [5]. However, the gross bony overgrowth found in melorheostosis with >70% genetically normal cells suggests that affected osteoblasts are influencing surrounding genotypically normal cells. VEGF is a soluble factor that is known to enhance endochondral bone formation [20]. VEGF has been shown to stimulate proliferation of human mesenchymal progenitor cells and osteoblasts, and is also reported to enhance osteoblast differentiation in a dose-dependent manner by elevating alkaline phosphatase activity and nodule formation [21–23]. Further evidence suggests that VEGF regulates bone homeostasis in mesenchymal progenitors and osteoblasts

through autocrine and intracrine signaling by increasing deposition of extracellular matrix, which is subsequently mineralized during bone formation [24,25]. Our findings illustrate the role of MEK1 hyperactivity in driving VEGF secretion in mesenchymal progenitor cell populations and differentiated osteoblasts. We further corroborate these findings with immunohistochemical staining of focal regions with elevated VEGF levels in melorheostotic bone andwith the demonstration that addition of VEGF results in increased mineralization of mutation-negative osteoblasts Because the phenotype of melorheostosis is so profound, it is likely that other secreted factors are involved as well.

In addition to the direct influence of VEGF on osteogenesis, several observations point to increased angiogenesis as a key driver of melorheostosis lesion progression. Micro-CT and histological examination of melorheostosis lesions show increased vascularity[3,26]. The coupling of angiogenesis and osteogenesis in intramembranous ossification is maintained through osteoblast-secreted VEGF recruitment of endothelial cells, which in turn release pro-osteogenic growth factors such as BMP-2 and BMP-4[24,27]. Supraphysiological VEGF levels have also been demonstrated to increase osteoclast recruitment, osteoclastic bone resorption, and overall bone turnover, which is consistent with the extensive remodeling and unmineralized osteoid found in histological examination of melorheostotic bone [19]. Previous work has shown that affected melorheostosis fibroblasts secrete greater amounts of collagens I and IV, which are known to support new vessel formation [14,28–30]. Similarly, we demonstrate heightened deposition of collagens I and IV in affected iMSCs, which may also contribute to neoangiogenesis within bone. Further exploration of osteoblast/endothelial cell interaction in the context of melorheostotic angiogenesis and bone formation is warranted, as the slow but continual progression of melorheostotic lesions without evidence of necrosis necessitates increased vessel recruitment.

In initial experiments with limited samples, we observed decreased mineralization in primary affected osteoblasts as compared to unaffected controls[5]. We believe this incongruency is attributable to limited availability and heterogeneity of samples. In the initial studies of melorheostosis, small bone samples were obtained because the effects of surgery were unknown. The mineralization experiments could only be performed with one 7-week time point. Histological study of melorheostosis has demonstrated variability in bone formation within the lesion (Figure 1), and this heterogeneity may have contributed to previous observations. With the availability of iPSC lines to perform multiple experiments as well as more patient samples, we have repeatedly observed increased mineralization in affected osteoblasts and affected patient-derived iMSCs, an observation more consistent with the clinical picture. A recent mouse model with increased MEK activation also showed an increased volume of bone by micro CT and stronger bone by biomechanical testing[10]. However, the mouse model is at a difference locus of the MAP2K1, does not fully replicate the candle wax bone formation seen in humans, and thus is not a perfect model.

A major limitation our study is that, while multiple patients' samples were started in the iPSC reprogramming process, only one cell line maintained the mutation. While some of the findings may only be present in this iPSC line, we confirmed the critical findings of VEGF secretion and bevacizumab inhibition in unrelated primary osteoblast samples.

Our study reports, for the first time, an iPSC-based model that recapitulates aberrant bone formation and mineralization in the context of melorheostosis. Assessment of rare diseases are frequently limited by a paucity of available patient cell lines, necessitating the development of iPSC-derived systems for interrogation of disease mechanisms and testing of possible therapeutic strategies [(31)]. Our findings suggest a central role of VEGF in stimulating pathological bone formation in melorheostosis and the potential of targeted VEGF neutralization in ameliorating disease progression. Further investigation of these phenomena in small-animal models of melorheostosis will be beneficial in developing therapeutic strategies. Given the rarity of osteosclerotic diseases, an understanding of the disease-causing MAP2K1 variant's role in bone formation may also provide mechanistic insights crucial to developing therapies for osteoporosis and related conditions.

CONCLUSION

We have established an iPSC-based model system to study the impact of melorheostosis-causing MAP2K1 mutations on osteoblast growth and differentiation. Our findings suggest that increased local VEGF secretion by affected osteoblasts plays a role in aberrant bone formation in melorheostosis. Further, we demonstrate the potential of targeted VEGF neutralization for inhibiting pathologic bone overgrowth.

Supplementary Material

Refer to Web version on PubMed Central for supplementary material.

ACKNOWLEDGEMENTS

This study was funded by NIAMS Intramural Research Program grant 1ZIDAR041180. The authors would also like to acknowledge Jeanette Beers of NHLBI the Institute for assistance with iPSC generation.

Data Availability Statement:

The data that support the findings of this study are available from the corresponding author upon reasonable request.

REFERENCES

1. Kerschan-Schindl K Romosozumab: a novel bone anabolic treatment option for osteoporosis? Wien Med Wochenschr. Apr 2020;170(5–6):124–31. Epub 20191219. [PubMed: 31858345]
2. Fick CN, Fratzl-Zelman N, Roschger P, Klaushofer K, Jha S, Marini JC, et al. Melorheostosis: A Clinical, Pathologic, and Radiologic Case Series. Am J Surg Pathol. Nov 2019;43(11):1554–9. [PubMed: 31386640]
3. Hoshi K, Amizuka N, Kurokawa T, Nakamura K, Shiro R, Ozawa H. Histopathological characterization of melorheostosis. Orthopedics. Mar 2001;24(3):273–7. [PubMed: 11300293]
4. Jha S, Cowen EW, Lehky TJ, Alter K, Flynn L, Reynolds JC, et al. Clinical Evaluation of Melorheostosis in the Context of a Natural History Clinical Study. JBMR Plus. Aug 2019;3(8):e10214. Epub 20190726. [PubMed: 31485554]
5. Kang H, Jha S, Deng Z, Fratzl-Zelman N, Cabral WA, Ivovic A, et al. Somatic activating mutations in MAP2K1 cause melorheostosis. Nat Commun. Apr 11 2018;9(1):1390. Epub 20180411. [PubMed: 29643386]

6. Jha S, Fratzl-Zelman N, Roschger P, Papadakis GZ, Cowen EW, Kang H, et al. Distinct Clinical and Pathological Features of Melorheostosis Associated With Somatic MAP2K1 Mutations. J Bone Miner Res. Jan 2019;34(1):145–56. Epub 20180914. [PubMed: 30138550]
7. Jha S, Ivovic A, Kang H, Meylan F, Hanson EP, Rimland C, et al. Distribution and Functional Consequences of Somatic MAP2K1 Variants in Affected Skin Associated with Bone Lesions in Melorheostosis. J Invest Dermatol. Mar 2021;141(3):688–92 e11. Epub 20200811. [PubMed: 32791068]
8. Arcila ME, Drilon A, Sylvester BE, Lovly CM, Borsu L, Reva B, et al. MAP2K1 (MEK1) Mutations Define a Distinct Subset of Lung Adenocarcinoma Associated with Smoking. Clin Cancer Res. Apr 15 2015;21(8):1935–43. Epub 20141028. [PubMed: 25351745]
9. Couto JA, Huang AY, Konczyk DJ, Goss JA, Fishman SJ, Mulliken JB, et al. Somatic MAP2K1 Mutations Are Associated with Extracranial Arteriovenous Malformation. Am J Hum Genet. Mar 2 2017;100(3):546–54. Epub 20170209. [PubMed: 28190454]
10. Fowlkes JL, Bunn RC, Ray PD, Kalaitzoglou E, Uppuganti S, Unal M, et al. Constitutive activation of MEK1 in osteoprogenitors increases strength of bone despite impairing mineralization. Bone. Jan 2020;130:115106. Epub 20191102. [PubMed: 31689526]
11. Marks JL, Gong Y, Chitale D, Golas B, McLellan MD, Kasai Y, et al. Novel MEK1 mutation identified by mutational analysis of epidermal growth factor receptor signaling pathway genes in lung adenocarcinoma. Cancer Res. Jul 15 2008;68(14):5524–8. [PubMed: 18632602]
12. Murugan AK, Dong J, Xie J, Xing M. MEK1 mutations, but not ERK2 mutations, occur in melanomas and colon carcinomas, but none in thyroid carcinomas. Cell Cycle. Jul 1 2009;8(13):2122–4. Epub 20090709. [PubMed: 19411838]
13. Waterfall JJ, Arons E, Walker RL, Pineda M, Roth L, Killian JK, et al. High prevalence of MAP2K1 mutations in variant and IGHV4–34-expressing hairy-cell leukemias. Nat Genet. Jan 2014;46(1):8–10. Epub 20131117. [PubMed: 24241536]
14. Hurley-Novatny AC, Allbritton-King JD, Jha S, Cowen EW, Colbert RA, Navid F, et al. Fibroblasts from Patients with Melorheostosis Promote Angiogenesis in Healthy Endothelial Cells through Secreted Factors. J Invest Dermatol. Sep 2022;142(9):2406–14 e5. Epub 20220219. [PubMed: 35189151]
15. Layh-Schmitt G, Lu S, Navid F, Brooks SR, Lazowick E, Davis KM, et al. Generation and differentiation of induced pluripotent stem cells reveal ankylosing spondylitis risk gene expression in bone progenitors. Clin Rheumatol. Jan 2017;36(1):143–54. Epub 20161118. [PubMed: 27864696]
16. Beers J, Linask KL, Chen JA, Siniscalchi LI, Lin Y, Zheng W, et al. A cost-effective and efficient reprogramming platform for large-scale production of integration-free human induced pluripotent stem cells in chemically defined culture. Sci Rep. Jun 11 2015;5:11319. Epub 20150611. [PubMed: 26066579]
17. Beers J, Gulbranson DR, George N, Siniscalchi LI, Jones J, Thomson JA, et al. Passaging and colony expansion of human pluripotent stem cells by enzyme-free dissociation in chemically defined culture conditions. Nat Protoc. Nov 2012;7(11):2029–40. Epub 20121025. [PubMed: 23099485]
18. Bullwinkel J, Baron-Luhr B, Ludemann A, Wohlenberg C, Gerdes J, Scholzen T. Ki-67 protein is associated with ribosomal RNA transcription in quiescent and proliferating cells. J Cell Physiol. Mar 2006;206(3):624–35. [PubMed: 16206250]
19. Street J, Bao M, deGuzman L, Bunting S, Peale FV, Jr., Ferrara N, et al. Vascular endothelial growth factor stimulates bone repair by promoting angiogenesis and bone turnover. Proc Natl Acad Sci U S A. Jul 23 2002;99(15):9656–61. Epub 20020712. [PubMed: 12118119]
20. Peng H, Usas A, Olshanski A, Ho AM, Gearhart B, Cooper GM, et al. VEGF improves, whereas sFlt1 inhibits, BMP2-induced bone formation and bone healing through modulation of angiogenesis. J Bone Miner Res. Nov 2005;20(11):2017–27. Epub 20050718. [PubMed: 16234975]
21. Yang YQ, Tan YY, Wong R, Wenden A, Zhang LK, Rabie AB. The role of vascular endothelial growth factor in ossification. Int J Oral Sci. Jun 2012;4(2):64–8. [PubMed: 22722639]

22. Deckers MM, Karperien M, van der Bent C, Yamashita T, Papapoulos SE, Lowik CW. Expression of vascular endothelial growth factors and their receptors during osteoblast differentiation. Endocrinology. May 2000;141(5):1667–74. [PubMed: 10803575]

23. Pons J, Huang Y, Arakawa-Hoyt J, Washko D, Takagawa J, Ye J, et al. VEGF improves survival of mesenchymal stem cells in infarcted hearts. Biochem Biophys Res Commun. Nov 14 2008;376(2):419–22. Epub 20080918. [PubMed: 18789891]

24. Grosso A, Burger MG, Lunger A, Schaefer DJ, Banfi A, Di Maggio N. It Takes Two to Tango: Coupling of Angiogenesis and Osteogenesis for Bone Regeneration. Front Bioeng Biotechnol. 2017;5:68. Epub 20171103. [PubMed: 29164110]

25. Hu K, Olsen BR. Vascular endothelial growth factor control mechanisms in skeletal growth and repair. Dev Dyn. Apr 2017;246(4):227–34. Epub 20161229. [PubMed: 27750398]

26. Fratzl-Zelman N, Roschger P, Kang H, Jha S, Roschger A, Blouin S, et al. Melorheostotic Bone Lesions Caused by Somatic Mutations in MAP2K1 Have Deteriorated Microarchitecture and Periosteal Reaction. J Bone Miner Res. May 2019;34(5):883–95. Epub 20190122. [PubMed: 30667555]

27. Hu K, Olsen BR. Osteoblast-derived VEGF regulates osteoblast differentiation and bone formation during bone repair. J Clin Invest. Feb 2016;126(2):509–26. Epub 20160105. [PubMed: 26731472]

28. Endo H, Katsumi A, Kuroda K, Utani A, Moriya H, Shinkai H. Increased procollagen alpha1(I) mRNA expression by dermal fibroblasts in melorheostosis. Br J Dermatol. Apr 2003;148(4):799–803. [PubMed: 12752142]

29. Li J, Zhang YP, Kirsner RS. Angiogenesis in wound repair: angiogenic growth factors and the extracellular matrix. Microsc Res Tech. Jan 1 2003;60(1):107–14. [PubMed: 12500267]

30. Newman AC, Nakatsu MN, Chou W, Gershon PD, Hughes CC. The requirement for fibroblasts in angiogenesis: fibroblast-derived matrix proteins are essential for endothelial cell lumen formation. Mol Biol Cell. Oct 2011;22(20):3791–800. Epub 20110824. [PubMed: 21865599]

31. Anderson RH, Francis KR. Modeling rare diseases with induced pluripotent stem cell technology. Mol Cell Probes. Aug 2018;40:52–9. Epub 20180105. [PubMed: 29307697]

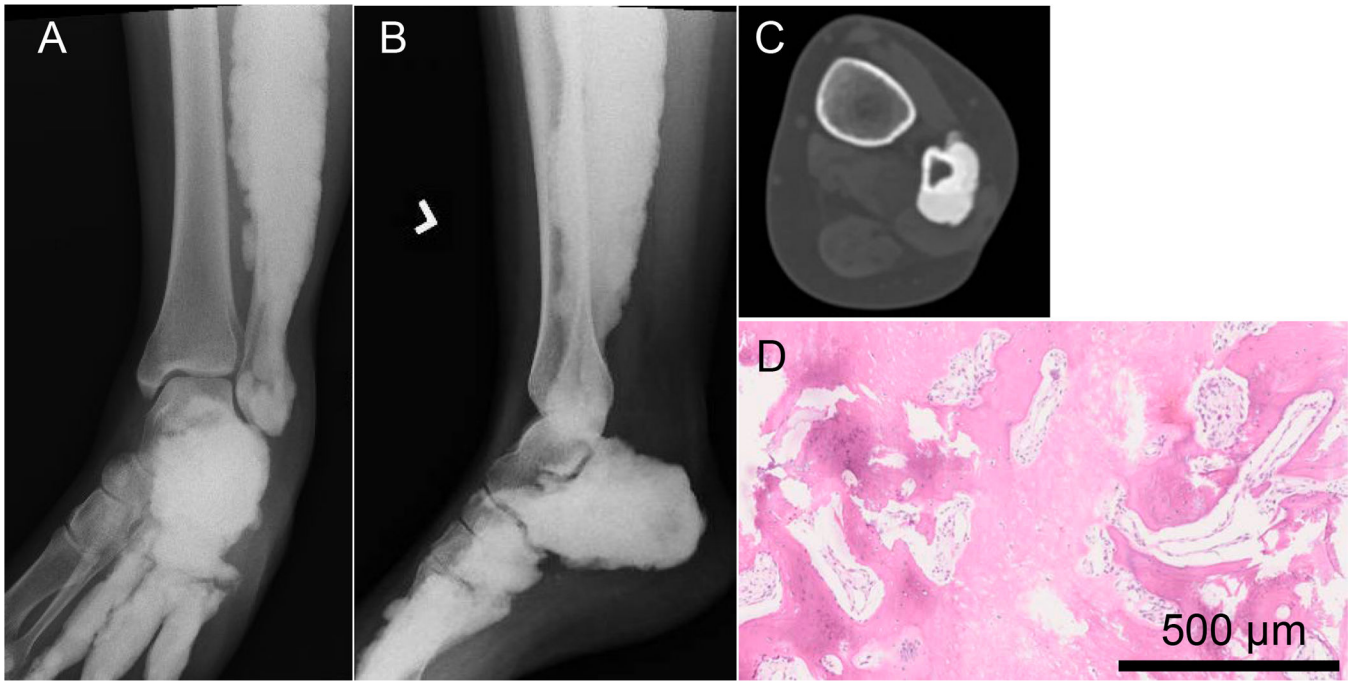

Figure 1. Clinical Findings in Melorheostosis.

AP (A) and Lateral (B) radiographs of a 42 year-old with classic melorheostosis (MAP2K1mutation positive). Candle wax bone formation is seen on the fibula calcaneus and lateral three rays. (C) CT scan reveals normal architecture of fibula with bony overgrowth. (D) H&E staining of affected bone reveals woven dense cortical-like bone with some variation in mineralization. Scale bar = 500 μm.

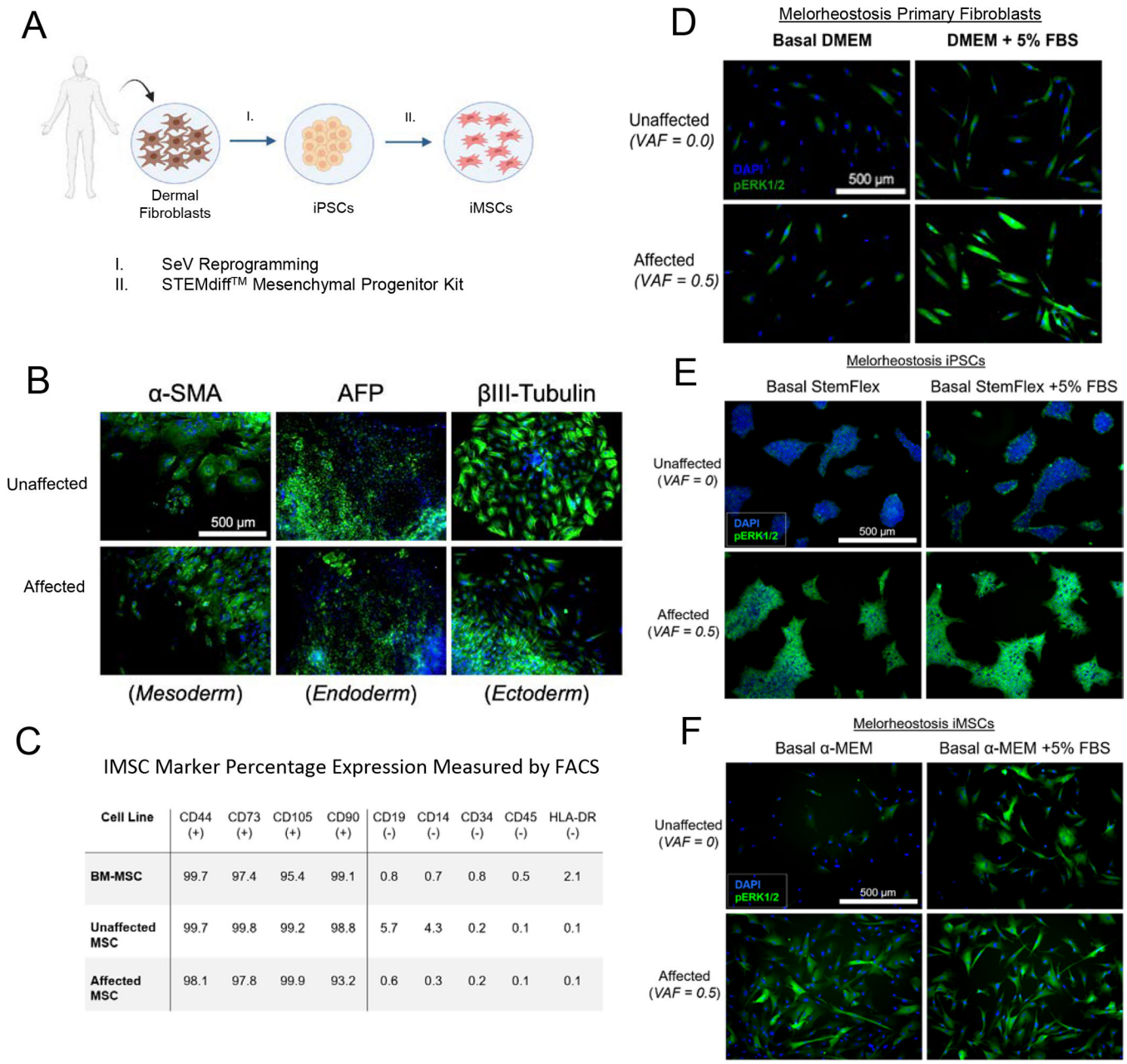

Cell Line	CD44 (+)	CD73 (+)	CD105 (+)	CD90 (+)	CD19 (-)	CD14 (-)	CD34 (-)	CD45 (-)	HLA-DR (-)
BM-MSC	99.7	97.4	95.4	99.1	0.8	0.7	0.8	0.5	2.1
Unaffected MSC	99.7	99.8	99.2	98.8	5.7	4.3	0.2	0.1	0.1
Affected MSC	98.1	97.8	99.9	93.2	0.6	0.3	0.2	0.1	0.1

Figure 2. Reprogramming and validation of MAP2K1 mutation activity in primary patient cells.

(A) Schematic of iPSC generation and iMSC differentiation from patient fibroblasts. (B) Embryoid body formation and germ layer staining for affected and unaffected patient iPSCs. (C) Flow cytometry validation of iMSC lineage markers of affected and unaffected patient iPSCs, with BM-MSC positive control. pERK1/2 activation in affected and unaffected (D) primary fibroblasts, (E) iPSCs, and (F) iMSCs in basal culture medium or 5% FBS stimulation. Scale bars = 500 µm.

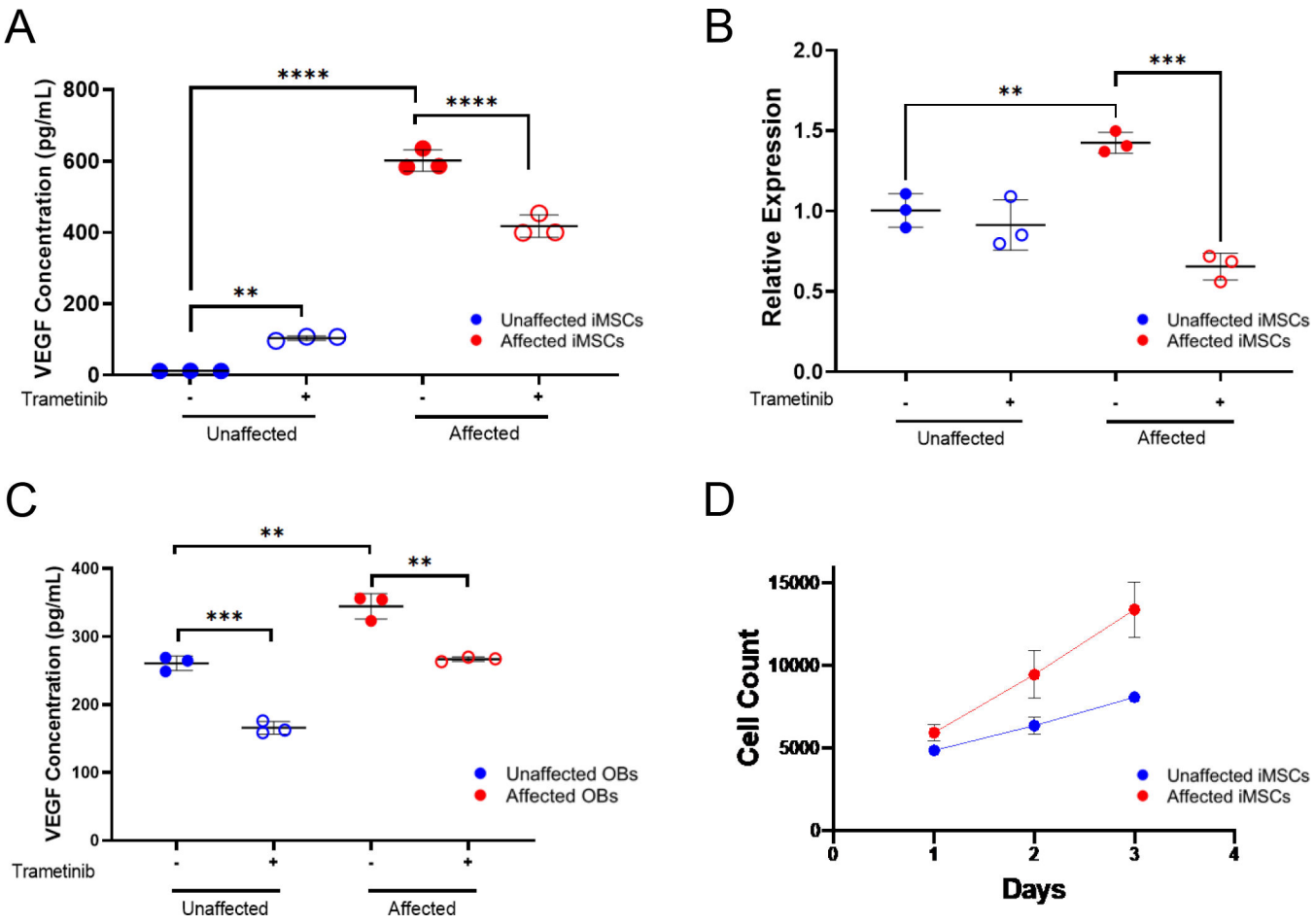

Figure 3. Affected iMSCs exhibit increased VEGF secretion.

(A) 48-hour secretion and (B) relative expression of VEGF from unaffected and affected iMSCs with or without 10uM of MEK inhibitor trametinib. (C) 48-hour secretion of VEGF from primary unaffected and affected osteoblasts with or without 10uM trametinib. (D) 72-hour proliferation curve of unaffected and affected iMSCs. All experiments were done in n=3 technical triplicates.

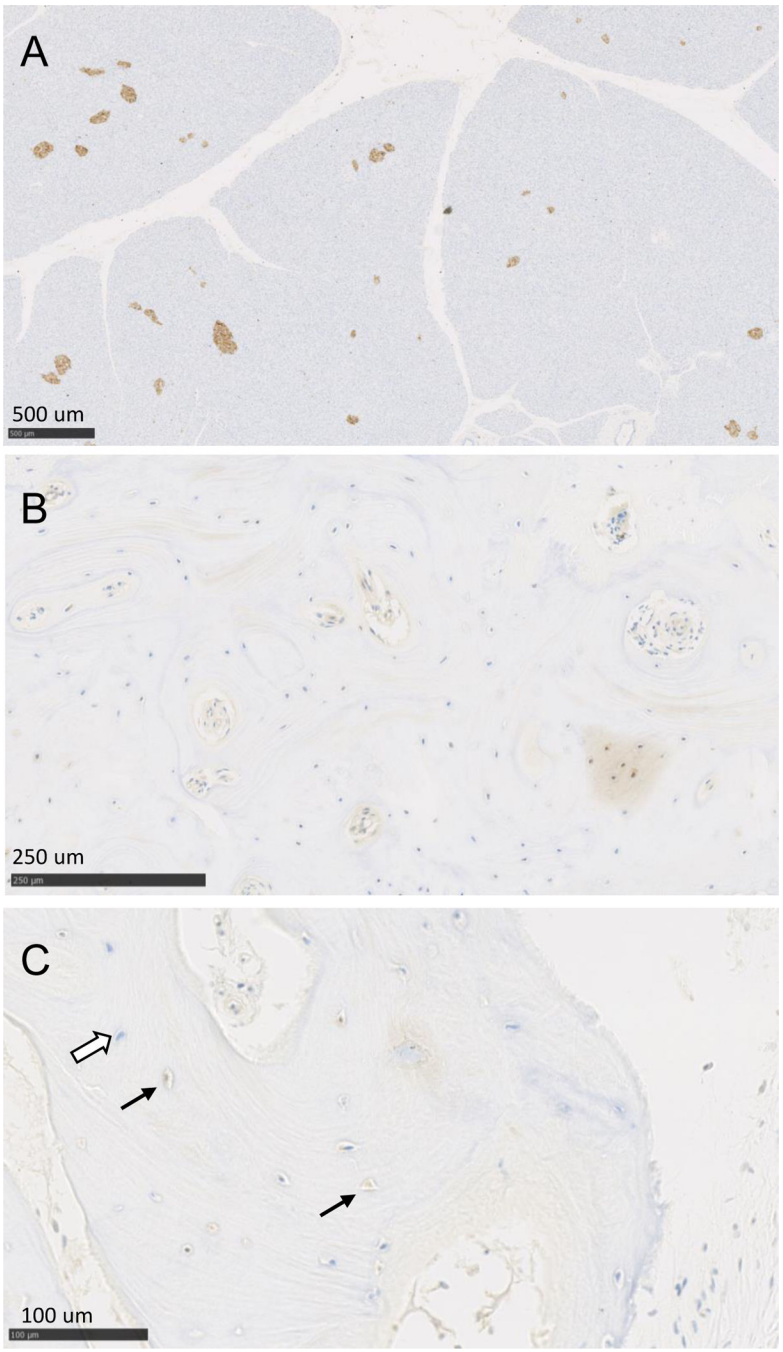

Figure 4. VEGF Immunohistochemistry in Melorheostosis Bone.

(A) Positive control VEGF staining of pancreas shows brown staining in the islet cells. Scale bar = 500 μm. (B) Immunohistochemistry of affected melorheostosis bone shows brown VEGF staining of pockets of osteocytes and Haversian canals. Scale bar = 250 μm. (C) Higher power view shows some osteocytes stain brown positive (solid arrows) while others are negative (empty arrow), consistent with a mosaic disease. Scale bar = 100 μm.

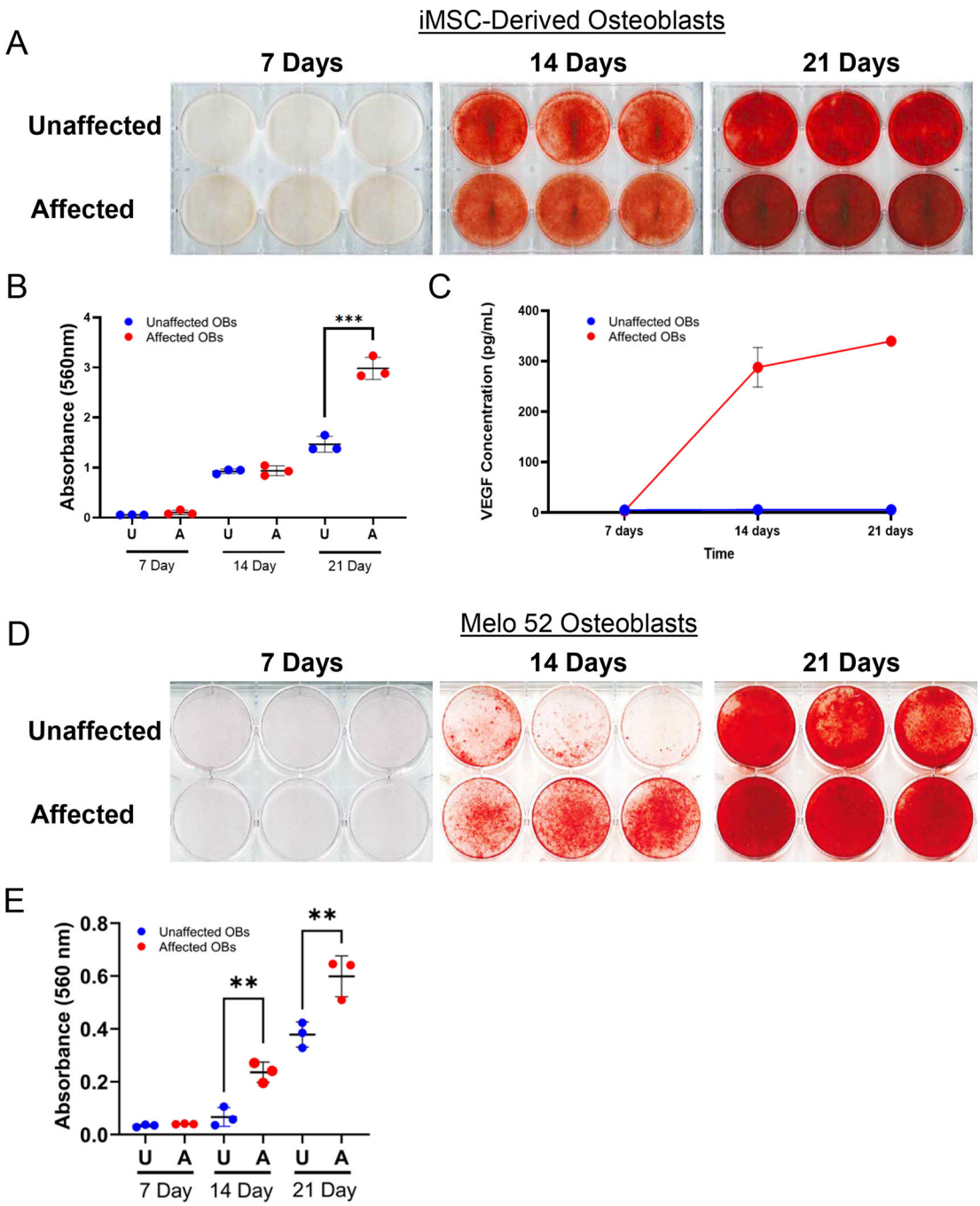

Figure 5. Affected iMSC and primary osteoblast hypermineralization in vitro.

(A) Alizarin red staining, (B) quantification, and (C) VEGF secretion of unaffected and affected iMSCs at 7, 14, and 21 days of osteogenic differentiation. (D) Alizarin red staining and (E) quantification of unaffected and affected primary osteoblasts at 7, 14, and 21 days of osteogenic differentiation. All experiments were done in n=3 technical triplicates.

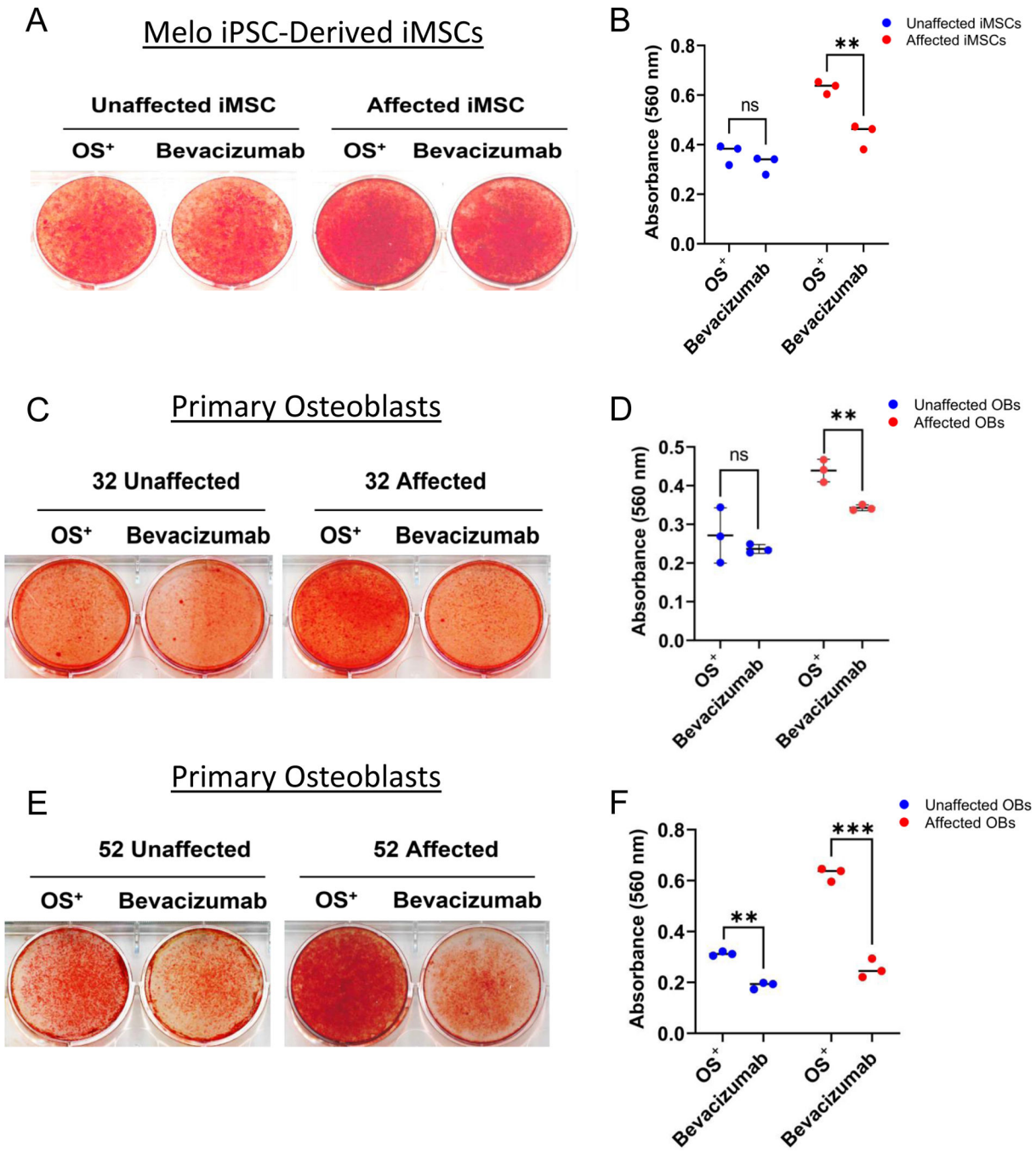

Figure 6. Bevacizumab inhibits mineralization in melorheostosis.

(D) Primary osteoblasts grown in osteogenic media with and without the VEGF inhibitor bevacizumab. (E) Quantification demonstrates decreased mineralization when affected cells were treated with bevacizumab. Findings were replicated in primary osteoblasts derived from another patient (E) and quantitated (F). All experiments were done in n=3 technical triplicates.